Experimental Investigation of the Effect of Oil on Steady-State Foam Flow in Porous Media

Tang, Jinyu; Vincent-Bonnieu, Sebastien; Rossen, William R.

DOI
10.2118/194015-PA

Publication date
2019

Document Version
Final published version

Published in
SPE Journal

Experimental Investigation of the Effect of Oil on Steady-State Foam Flow in Porous Media

Jinyu Tang*, Delft University of Technology; **Sebastien Vincent-Bonnieu,** Delft University of Technology and Shell Global Solutions International; and **William R. Rossen,** Delft University of Technology

Summary

Foam flow in porous media without oil shows two regimes depending on foam quality (gas fractional flow). Complexity and limited data on foam/oil interactions in porous media greatly restrict understanding of foam in contact with oil. Distinguishing which regimes are affected by oil is key to modeling the effect of oil on foam. We report steady-state corefloods to investigate the effect of oil on foam through its effect on the two flow regimes. We fit the parameters of a widely used local-equilibrium (LE) foam model to data for concurrent foam/oil flow. This research provides a practical approach and initial data for simulating foam enhanced oil recovery (EOR) in the presence of oil.

To ensure steady state, oil is coinjected with foam at a fixed ratio of oil (U_o) to water (U_w) superficial velocities in a Bentheimer Sandstone core. Model oils used here consist of a composition of hexadecane, which is benign to foam stability, and oleic acid (OA), which can destroy foam. Varying the concentration of OA in the model oil allows one to examine the effect of oil composition on steady-state foam flow. Experimental results show that oil affects both high- and low-quality regimes, with the high-quality regime being more sensitive to oil. In particular, oil increases the limiting water saturation (S_w^*) in the high-quality regime and also reduces gas-mobility reduction in the low-quality regime. Unevenly spaced ∇p contours in the high-quality regime suggest either strongly shear-thinning behavior or an increasingly destabilizing effect of oil. In some cases, the pressure gradient (∇p) in the low-quality regime decreases with increasing U_w at fixed gas superficial velocity (U_g), either with or without oil. This might reflect either an effect of oil, if oil is present, or easier flow of bubbles under wetter conditions. Increasing the OA concentration extends the high-quality regime to lower foam qualities, indicating more difficulty in stabilizing foam. Thus, oil composition plays as significant a role as oil saturation (S_o).

A model fit assuming a fixed S_w^* and including shear thinning in the low-quality regime does not represent the two regimes when the oil effect is strong enough. In such cases, fitting S_w^* to each ∇p contour and excluding shear thinning in the low-quality regime yield a better match to these data. The dependency of S_w^* on S_o is not yet clear because of the absence of oil-saturation data in this study. Furthermore, none of the current foam-simulation models captures the upward-tilting ∇p contours in the low-quality regime.

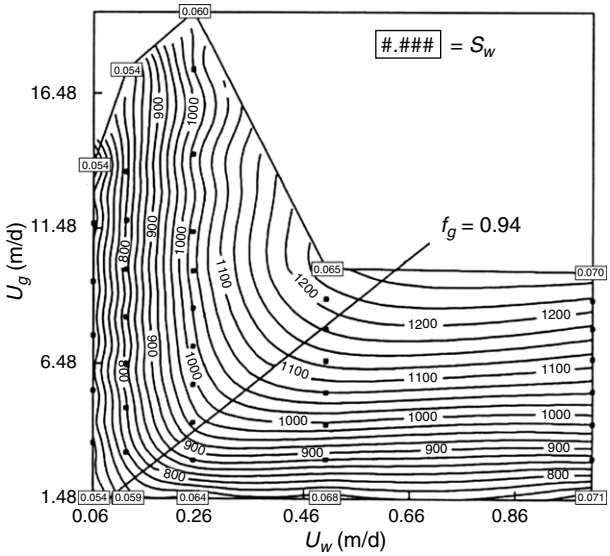

Fig. 1—Pressure drop across a 2-ft sandpack as a function of superficial velocities of gas (U_g) and water (U_w). The pressure gradient, in psi/ft, is one-half the values listed. The contours of equal pressure drop are plotted through steady-state data represented by black points, from Osterloh and Jante (1992). The high-quality regime is to the upper left and the low-quality regime is on the lower right.

Introduction

Numerous laboratory studies and field pilots demonstrate that steady-state foam flow comprises two regimes depending on foam quality (gas fractional flow) (Osterloh and Jante 1992; Alvarez et al. 2001): the high-quality (or coalescence) regime, which is dominated by foam stability, and the low-quality (or wet) regime, in which foam strength is controlled by a mobility-reduction factor (MRF). **Fig. 1**

* corresponding author, email: J.Tang-4@tudelft.nl

Original SPE manuscript received for review 11 December 2017. Revised manuscript received for review 17 April 2018. Paper (SPE 194015) peer approved 4 July 2018.

illustrates this behavior. These two regimes are central to our understanding of foam without oil and also modeling of foam with oil, but this fundamental property is identified in the absence of oil. Because of the limited data available and the complexity of foam/oil interactions, the effect of oil on foam is not fully understood yet. This knowledge gap greatly limits our ability to represent the effect of oil on foam in modeling (Harkins and Feldman 1922; Bergeron et al. 1993; Farajzadeh et al. 2012), in particular its effect on the two regimes central to our understanding of foam without oil. The effectiveness of foam in the presence of oil is key to successful application of foam for EOR. This issue hinders the reliable design of foam processes and effective prediction of foam performance.

Prior work on foam/oil interactions has identified some surface phenomena and proposes some coefficients to represent them (Farajzadeh et al. 2012): the entering coefficient (Bergeron et al. 1993), the spreading coefficient (Harkins and Feldman 1922), the bridging coefficient (Aveyard et al. 1994), and the lamella number (Schramm and Novosad 1990, 1992). These coefficients can serve to represent the effects of oil on foam in bulk. However, foam behavior identified in bulk is not necessarily consistent with that in porous media. In some cases, foam behavior in these two scenarios is contradictory. Besides, none of these coefficients is by itself a sufficient criterion for judging the stability of foam interacting with oil (Basheva et al. 2000). Moreover, these coefficients do not quantitatively predict the effect of oil on foam.

Some studies (Andrianov et al. 2011; Zanganeh et al. 2011) on the effect of oil on foam indicate that most oils are detrimental to foam stability, and the lighter (also less viscous) the oil, the more harmful it is to foam. However, as discussed previously, there is no quantitative predictive model for the effect of oil on foam. Studies have shown that foam is destroyed when the oil saturation is greater than a critical oil saturation (Mannhardt et al. 1998). This critical oil saturation is used to model the oil effect on foam, as in the LE implicit-texture (IT) model detailed in the Foam Models subsection. The critical oil saturation depends on the oil, rock, and surfactant chemistry. For example, a critical oil saturation of 0.2 or 0.3 was used for the history matching of the Snorre Field pilot (Spirov et al. 2012). However, no data on foam/oil interactions in steady-state flow are documented in the literature. Therefore, oil parameters taken in simulating foam for EOR processes might not reflect the actual situation in the field.

A modeling study on the effect of oil on foam (Tang et al. 2016) illustrates that foam/oil-interaction parameters in current foam models each shift one or the other of the two regimes. Depending on the model, the presence of oil shifts pressure-gradient (∇p) contours in the high-quality regime to the right, indicating an increase in limiting water saturation, below which foam collapses. Oil can also shift ∇p contours in the low-quality regime upward, reflecting reduced resistance to bubble flow. Our goal here is to measure the effect of oil on foam in the laboratory to see whether the effect of oil can be represented by these models. Specifically, this study examines the effect of oil on foam through its effect on the two regimes initially identified in the absence of oil. A series of corefloods were performed by applying coinjection of foam and oil, with oil injected at a fixed ratio of oil superficial velocity (U_o) to water superficial velocity (U_w). Through this injection strategy, the effect of oil can be quantified. To examine the effect of oil composition on foam, for simplicity, two oil components were selected: one component is less destructive to foam (Simjoo and Zitha 2013) and the other component can destroy foam completely. Varying the proportion of these two oil components in the model oil allows one to examine the effect of oil composition on foam stability in porous media.

Then, applying a method similar to that of Cheng et al. (2000), for the first time, we fit an LE IT foam model, adapted from the widely used STARS model (CMG 2015), to experimental data for LE foam flow in the presence of oil. (The acronym "LE" means that the generation and destruction rates of bubbles approach a balance immediately.) This research provides a practical approach for measuring the effect of oil on foam in porous media. Initial data on foam/oil interactions obtained in this study give further insights for simulating foam for EOR in the presence of oil. In addition, these data can serve as a case study for representing the behavior of foam in contact with oil, and can enhance the reliability of a foam-process design.

Foam Models. Current foam models generally fall into two groups: population-balance models, characterizing the dynamics of bubble generation and destruction coupled with gas mobility represented as a function of bubble size (Friedmann et al. 1991; Kovscek et al. 1995; Rossen 1996; Kam et al. 2007), and IT models, capturing the effects of physical factors on LE foam flow [e.g., surfactant concentration, water saturation, oil saturation, salinity, and capillary number (Islam and Farouq Ali 1988; Kular et al. 1989; Patzek and Myhill 1989; Fisher et al. 1990; Law et al. 1992; Mohammadi et al. 1993; Cheng et al. 2000)]. Myers and Radke (2000) attempted to incorporate the effect of oil on foam in a population-balance model. However, the effect of oil in their study is modeled by simply reducing the bubble-generation rate, accounting for the blockage of generation sites by the presence of residual oil. This approach is not sufficient to capture the actual interaction dynamics of foam and oil (e.g., the effects of oil saturation and composition, or the stability and strength of foam with oil), which are crucial for better understanding the fundamentals of foam with oil in porous media. This study focuses on fitting the IT model parameters to experimental data.

In the LE IT foam model studied here, foam reduces gas mobility by modifying gas relative permeability with a mobility factor (FM),

$$k_{rg}^{f} = k_{rg}^{0} \times FM, \quad (1)$$

$$FM = \frac{1}{1 + fmmob \times F_1 \times F_2 \times F_3 \times F_4 \times F_5 \times F_6 \ldots}, \quad (2)$$

where *fmmob,* the reference gas MRF, is defined as the maximum-attainable gas-mobility reduction, and F_1 through F_6 are functions accounting for the effects of physical factors on gas mobility (e.g., surfactant concentration, water saturation, oil saturation, oil composition, capillary number, and salinity). Here, we consider three functions, F_2, F_3, and F_5, capturing the effects of water saturation, oil saturation, and shear thinning, respectively, in the low-quality regime. The foam model used includes two algorithms for the effect of oil on foam: the wet-foam model and the dry-out model.

In the wet-foam model, F_2 represents the effect of water saturation on gas mobility,

$$F_2 = 0.5 + \frac{\arctan[epdry(S_w - fmdry)]}{\pi}, \quad (3)$$

where *epdry* controls the abruptness of foam collapse as water saturation decreases to less than the limiting water saturation, *fmdry,* around which foam collapses. If *epdry* is large, separate sets of parameters affect the high- and low-quality regimes (Cheng et al. 2000). The value of *fmdry* is usually assumed to be fixed throughout the high-quality regime (Cheng et al. 2000; Boeije and Rossen 2015). This parameter is renamed as *sfdry* in the dry-out model. To avoid confusion, the limiting water saturation is mostly referred to here by its physical denotation, S_w^*.

In the foam model, the effect of oil is restricted by the upper and lower limiting oil saturations, distinguishing the oil saturation above which oil starts harming foam and above which oil completely destroys foam. Oil saturation specifically affects foam in the wet-foam model through scaling the reference MRF *fmmob* with

$$F_3 = \begin{cases} 1, & S_o \le floil \\ \left(\dfrac{fmoil - S_o}{fmoil - floil}\right)^{epoil}, & floil < S_o < fmoil \\ 0, & fmoil \le S_o \le 1 - S_{wc} - S_{gr} \end{cases}, \quad \ldots\ldots (4)$$

where *floil* and *fmoil* are oil-related parameters marking the boundaries when oil destabilizes and destroys foam, respectively, and *epoil* is the oil exponent.

F_5, capturing shear-thinning behavior in the low-quality regime, is given by

$$F_5 = \begin{cases} \left(\dfrac{fmcap}{N_{ca}}\right)^{epcap}, & N_{ca} \ge fmcap \\ 1, & \text{else} \end{cases}, \quad \ldots\ldots (5)$$

$$N_{ca} \equiv \frac{k\nabla p}{\sigma_{wg}}, \quad \ldots\ldots (6)$$

where *fmcap* and *epcap* are model parameters and N_{ca} is the capillary number, defined as a product of absolute permeability k multiplied by the pressure gradient and divided by the water/gas surface tension.

In the dry-out model, oil affects gas mobility not by scaling *fmmob* but by modifying the limiting water saturation S_w^*. F_2 in the dry-out model is rewritten as F_7, given by

$$F_7 = 0.5 + \frac{\arctan[sfbet(S_w - sfdry)]}{\pi}, \quad \ldots\ldots (7)$$

where *sfbet* and *sfdry* play the same roles of *epdry* and *fmdry* in the wet-foam model, respectively. However, *sfdry* is not a constant in this model, but instead depends on oil saturation through function G_2 (similar to function F_3 in the wet-foam model):

$$[(1 - sfdry) \times G_2 + sfdry] \rightarrow sfdry, \quad \ldots\ldots (8)$$

$$G_2 = \begin{cases} 0, & S_o \le sloil \\ \left(\dfrac{S_o - sloil}{sfoil - sloil}\right)^{efoil}, & sloil < S_o < sfoil \\ 1, & sfoil \le S_o \le 1 - S_{wc} - S_{gr} \end{cases}, \quad \ldots\ldots (9)$$

where oil-related parameters *sloil, sfoil,* and *efoil* correspond to *floil, fmoil,* and *epoil* in the wet-foam model, respectively.

Tang et al. (2016) show that the wet-foam model represents the effect of oil only on the low-quality regime, whereas the dry-out model captures the effect of oil only on the high-quality regime. However, these results indicate only the effect of oil on foam as represented by this model. The experimental data shown in the following subsections clearly demonstrate which regimes are affected by oil and serve to check the suitability of the model. The procedures for fitting the model parameters to data are further discussed in Appendix B.

Experimental Method. ***Experimental Scheme.*** To examine the effect of oil on LE foam flow in cores, first a series of pure hydrocarbons were screened using bulk-foam tests and coreflood evaluation to select two oil components with a range of effects on foam. In particular, we wanted one component that destabilizes foam slightly and another that substantially destroys foam. The surfactant used is sodium alpha-olefin-sulfonate at a concentration of 0.5 wt%, with a salinity of 3 wt% sodium chloride. More details regarding the materials used can be found in the Apparatus and Materials subsection. In the bulk-foam test, 5 cm^3 of surfactant solution was mixed in a 10-cm^3 test tube with 1 cm^3 of different pure alkanes (e.g., C_{16}, C_{14}, C_{12}, C_{10}, C_9, C_8, and C_6). These test tubes were kept in an oven at 35°C to check if surfactant precipitates in contact with these alkanes. Foam then is generated by manually shaking these test tubes. The bulk-foam tests here were used to roughly characterize the defoaming potential of a variety of pure alkanes in terms of surfactant precipitation, initial foam height, and foam decay over time. This method can give a quick screening of the detrimental effect of the examined hydrocarbons. Because foam behavior in bulk is not always consistent with that in porous media, several candidates potentially meeting our expectations were examined again with corefloods for MRF. MRF is defined here as a ratio of pressure drop with foam to that with brine-only injection at the same total superficial velocity,

$$MRF = \frac{\Delta p_{fm}}{\Delta p_{nf}}, \quad \ldots\ldots (10)$$

where Δp_{fm} and Δp_{nf} denote the pressure drop with and without foam, respectively.

All corefloods in this study were conducted in Bentheimer sandstone at 35°C with a backpressure fixed at 50 bar. The same core was used to guarantee consistency of experiments. To reuse the core, we cleaned the core by flushing it with, in order, isopropanol, carbon dioxide (CO_2), and water. Backpressure is then increased and reduced during water flushing to dissolve and remove CO_2 in the system. Two oil components were then selected combining the evaluation results of the bulk-foam tests and the initial screening corefloods. Before performing foam corefloods in the presence of oil, a set of experiments without oil was conducted first to identify the two regimes. These two regimes serve as a reference for comparing the effect of oil. During corefloods, instead of monotonically increasing or reducing gas (U_g) or water (U_w) superficial velocity, U_g and U_w were varied in a random sequence to avoid confusing any permeability loss over time with the effect of foam quality. Thereafter, a series of foam corefloods were conducted, with oil coinjected concurrently, to examine steady-state interaction of foam and oil in porous media. Specifically, to measure the oil effect quantitatively and to ensure steady state, foam was coinjected with oil at a fixed ratio R of oil (U_o) to water (U_w) superficial velocity. The variation in U_w therefore means a proportional change in U_o. We did not measure oil or water saturation in our experiments, so they were estimated

through relative permeability functions. Therefore, it is not practical here to directly quantify foam mobility as a function of oil saturation. Varying the proportion of the two oil components selected allows one to investigate the effect of oil composition on the two regimes central to our understanding of foam without oil.

Apparatus and Materials. The injection system here allows for coinjection of three phases (water, oil, and gas) through two pumps for oil and surfactant solution, respectively, and a gas-mass-flow controller, as shown in **Fig. 2.** The core holder is equipped with five pressure taps for monitoring the pressure drop across each section along the core during corefloods. The gap between the core and the core holder is connected with the inlet line to impose confining pressure. The whole core holder is placed in a water bath maintained at 35°C. The pressure data are recorded by the data-acquisition system through LabVIEW (Elliott et al. 2007). The backpressure regulator allows us to perform experiments under elevated pressure and maintains stable outlet pressure.

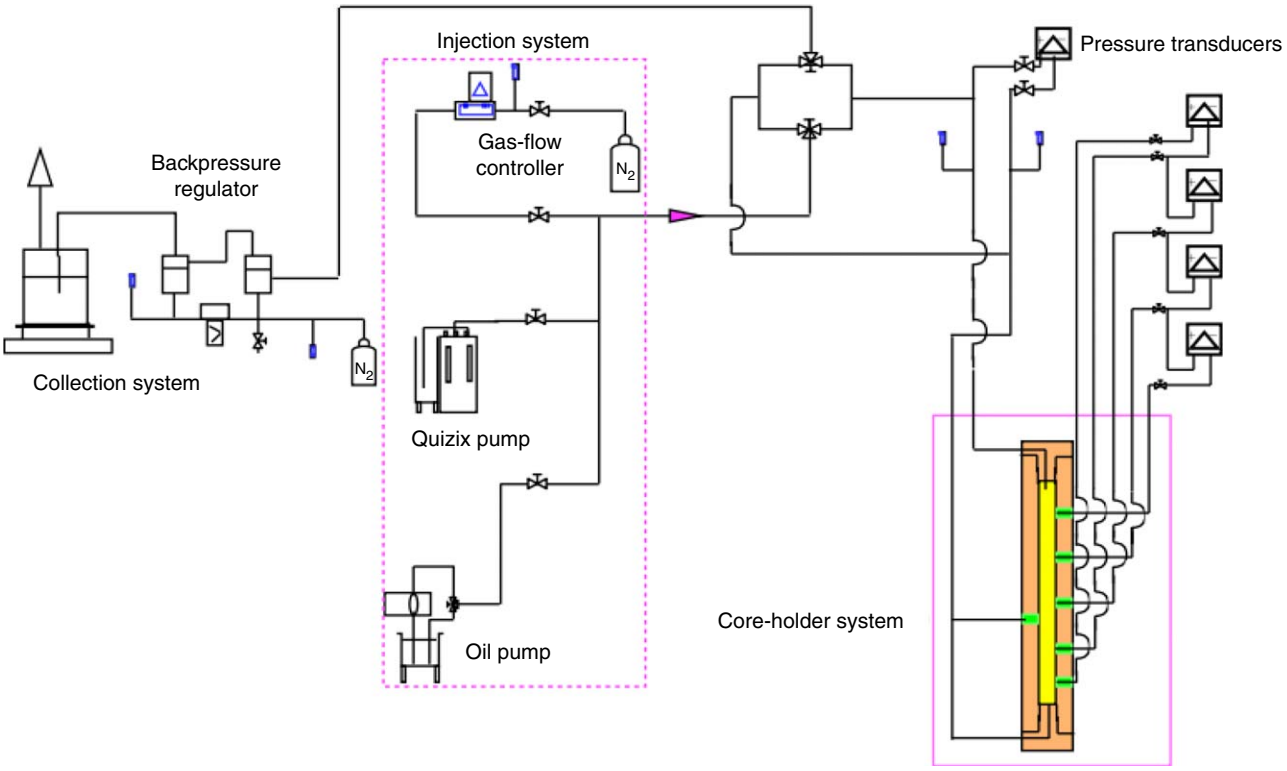

Fig. 2—A schematic overview of the apparatus used for steady-state foam corefloods, allowing for concurrent coinjection of oil, water, and gas.

All corefloods conducted here were performed in a Bentheimer core that was 4 cm in diameter and 40 cm in length, with an absolute permeability of 1.98 darcies. The foaming agent used is sodium $C_{14–16}$ olefin sulfonate BIO-TERGE AS-40K with an activity of 40%, from Stepan Company. Sodium chloride is the only salt used to provide salinity, which is 30,000 ppm in all experiments. To screen the oils for experimental study, pure hydrocarbons and OA are examined: hexadecane (C_{16}), tetradecane (C_{14}), dodecane (C_{12}), decane (C_{10}), nonane (C_9), octane (C_8), and hexane (C_6). The gas injected is nitrogen. OA ($C_{18}H_{34}O_2$) with 99% purity was from Honeywell Fluka in the Netherlands. All the alkanes are provided by Sigma-Aldrich, with a purity of 99% for each.

In laboratory corefloods, a region near the inlet and a region close to the outlet might reflect an entrance or the capillary end effect, respectively. To minimize these effects, all the experimental results reported in the following section are derived from data from the third section among the four sections monitored along the flow direction. Most of the time, when the pressure drops for the two middle sections are approximately equal and stable with acceptable fluctuations, it is assumed to be a steady state for each measurement. For those injection conditions under which nonuniform state is achieved, we take the data of the second of the middle two sections.

Results

Oil Screening. Comparing foam decay over time with and without oil in the bulk-foam test, in terms of foam height and texture, shows that hexadecane slightly destabilizes foam. After 1,010 minutes, foam height decays by less than one-half, but foam texture is coarse. However, for all the rest of the alkanes examined, foam completely collapsed after 230 minutes, and the fewer the carbon atoms on the backbone, the more quickly the foam decayed.

Given the concern regarding inconsistency between foam behavior in bulk and in rock, C_{16}, C_{10}, C_8, and C_6 were examined again through corefloods in Bentheimer Sandstone. The MRF with and without oil in **Fig. 3** shows that hexadecane (C_{16}), consistent with the bulk-foam test, is relatively benign to foam stability. However, C_{10}, C_8, and C_6 are not so effective at destroying foam in porous media, although they are detrimental to foam stability in bulk. OA, however, destroys foam almost completely.

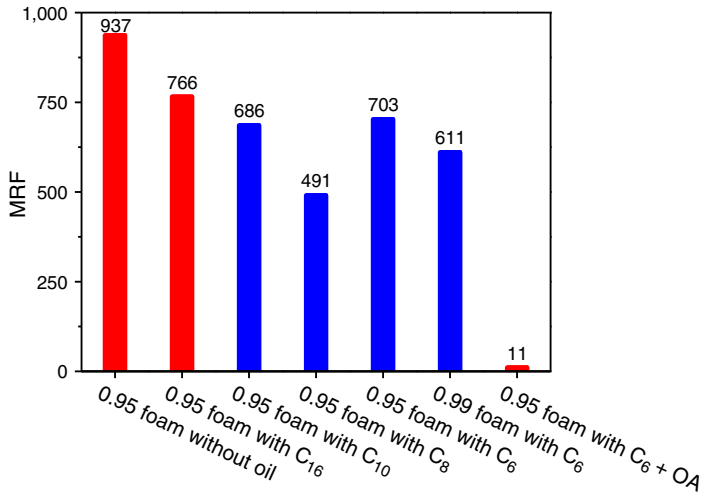

Fig. 3—Gas MRF as a function of oil type. Oil is coinjected with foam at a constant U_o/U_w ratio = 1/4 in a Bentheimer core of 1.98 darcies. The total superficial velocity of U_w and U_g is fixed at 1.5 m/d. Foam quality (0.95 or 0.99) in this case is defined as $f_g = U_g/(U_g + U_w)$. The oil used in the last case consists of 10% OA and 90% C_6.

The MRF with various oils in Fig. 3 appears to contradict the conclusion that the lighter the oil, the more detrimental it is to foam, in contrast to Andrianov et al. (2011) and Zanganeh et al. (2011). This issue is not addressed further here. The major intention of Fig. 3 is a quick screening to determine one oil component that can destroy foam for use in the subsequent experiments. Taking these results into account, hexadecane and OA were chosen as the two oil components: hexadecane as the one relatively benign to foam stability, and OA as the one destroying foam completely. **Fig. 4** shows that foam strength decreases greatly with increasing concentration of OA in the model oil. To partly destroy foam but still maintain some foam strength, model oils with 10 and 20 wt% OA were investigated. All experiments were conducted in the same core. To avoid the interference of oils used previously, we conducted experiments first without oil and then with C_{16}, 10% OA, and 20% OA in model oil, respectively.

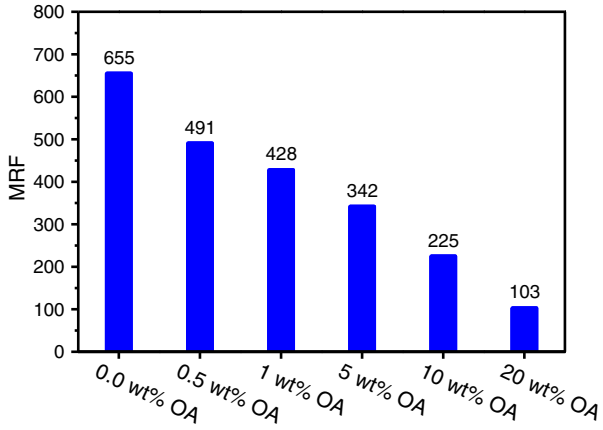

Fig. 4—The effect of OA concentration on foam strength at a foam quality of 0.95 in a Bentheimer core of 1.92 darcies. Foam quality in this case is defined as $U_g/(U_g + U_w)$. The total superficial velocity of U_w and U_g is fixed at 1.5 m/d. Oil is coinjected with foam at a constant U_o/U_w ratio = 1/4. The model oil consists of OA and C_{16}.

Two Foam Regimes With and Without Oil. ***LE Foam Flow Without Oil.*** **Fig. 5** demonstrates that steady-state foam flow in the absence of oil in a Bentheimer core shows two regimes, as expected. The high-quality regime appears at foam qualities greater than approximately 80%. The nearly vertical contours in this regime indicate the independence of ∇p from U_g. The pressure gradient increases from approximately 100 to 500 to 600 psi/ft upon doubling U_w from 0.13 to 0.25 ft/D, indicating strongly shear-thickening rheology in the high-quality regime.

However, the ∇p contours in the low-quality regime in Fig. 5, instead of appearing horizontal as in Fig. 1, tilt upward to the top right. This means that ∇p in the low-quality regime decreases with increasing U_w at fixed U_g. The studies of de Vries and Wit (1990) and Kim et al. (2005) on CO_2 foam in a variety of porous media suggest similar behavior in the low-quality regime. The study of Hirasaki and Lawson (1985) on foam-apparent viscosity in smooth capillaries and the study of Kim et al. (2005) on LE CO_2 foam suggest that this behavior might arise from easier flow of bubbles under wetter conditions. Specifically, increasing U_w in the low-quality regime implies an increase in water saturation; there are thicker water films around the bubbles, and there is therefore less flow resistance (less drag on bubble flow). This consequently yields lower ∇p at higher U_w at fixed U_g. More efforts are needed to examine the exact mechanism for upward-tilting ∇p contours in the low-quality regime.

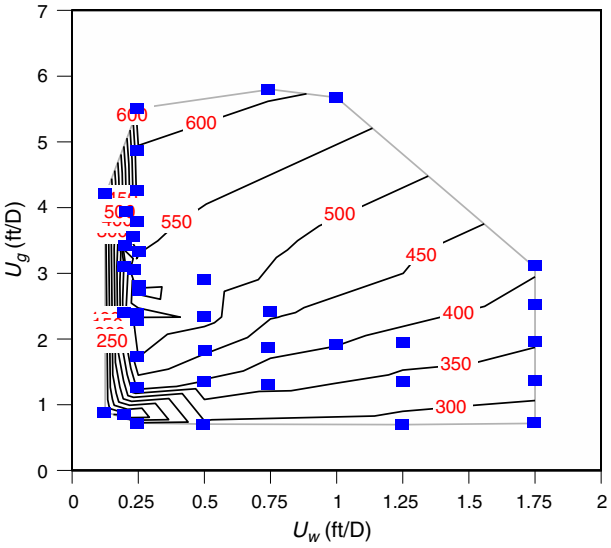

Fig. 5—Pressure gradient (in psi/ft) in the absence of oil, as a function of gas (U_g) and water (U_w) superficial velocities (in ft/D) at 35°C in a Bentheimer core of 1.98 darcies. Individual data are indicated by blue symbols. Each filled symbol here represents a steady-state measurement.

LE Foam Flow With C_{16}. **Fig. 6** shows that steady-state concurrent foam/oil flow (C_{16} in this case) still produces the two flow regimes as identified in the absence of oil: high- and low-quality regimes. Although hexadecane only slightly destabilizes foam in the bulk-foam tests, apparently both high- and low-quality regimes are affected by the presence of this oil. For the same range of U_g and U_w examined in Fig. 5, ∇p in the presence of C_{16} in Fig. 6 is restricted to less than approximately 220 psi/ft, nearly three times lower than that without oil (600 psi/ft) in Fig. 5.

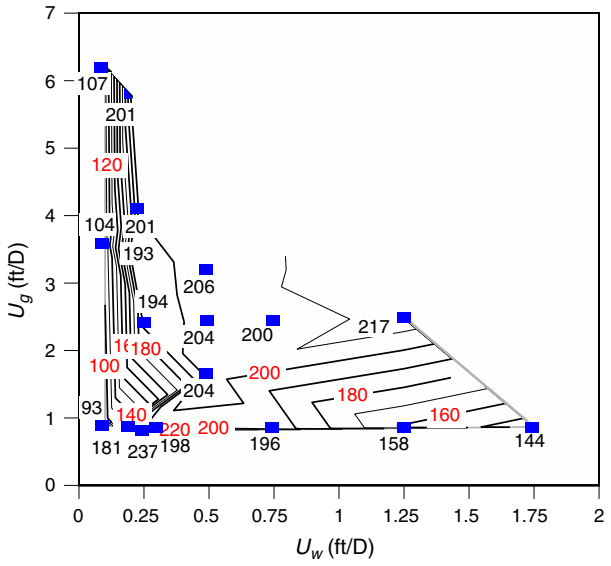

Fig. 6—Pressure gradient (in psi/ft) in the presence of oil, as a function of gas (U_g) and water (U_w) superficial velocities (in ft/D) at 35°C in a Bentheimer core of 1.98 darcies. Individual data are indicated by blue symbols. The oil used is hexadecane, coinjected with foam at a fixed U_o/U_w ratio = 1/4. Each filled symbol represents a steady-state measurement.

The high-quality regime in Fig. 6 shifts to the right compared with Fig. 5. This suggests that oil reduces foam stability in the high-quality regime by increasing the limiting water saturation (S_w^*) below which foam collapses. As shown in an expanded view of Fig. 6 in Appendix A, the uniform spacing of ∇p contours in this regime demonstrates nearly Newtonian rheology, reflecting an approximately constant S_w^*. The low-quality regime in Fig. 6 shifts to lower foam qualities compared with Fig. 5 (less than approximately 0.75). The ∇p in the low-quality regime is less than the ∇p in Fig. 5 by a factor of approximately two, a lesser reduction than in the high-quality regime. In addition, ∇p contours in the low-quality regime of Fig. 6, similar to those in Fig. 5, also tilt upward with increasing U_w. Because foam in this case is flowing together with oil, the upward-tilting ∇p contours might reflect easier flow of bubbles under wetter conditions, the destabilizing effect of oil on foam strength, or a combination of both effects.

The greater decrease in gas-mobility reduction in the high-quality regime than in the low-quality regime reveals that foam in the high-quality regime is more vulnerable to oil. For instance, in the high-quality regime of Fig. 6 with C_{16}, $(U_w, U_g) = (0.2, 2)$ gives a ∇p of 160 psi/ft, which is 2.5 times lower than 400 psi/ft, the ∇p obtained with the same set of flow rates in Fig. 5 without oil. In the low-quality regime, for $(U_w, U_g) = (1, 1.5)$, the ∇p in Fig. 6 yields 190 psi/ft, which is approximately 1.9 times lower than 360 psi/ft obtained with the same set of flow rates in Fig. 5.

LE Foam Flow With 10 wt% OA in Model Oil. Introduction of OA, although only 10 wt% in the model oil, plays a significant role on foam behavior and leads to some new behavior. **Fig. 7** illustrates that only the high-quality regime has been observed for the same range of U_w and U_g as examined in Figs. 5 and 6. The generally vertical trend of ∇p contours in the high-quality regime of Fig. 7 suggests that S_w^* is still independent of U_g.

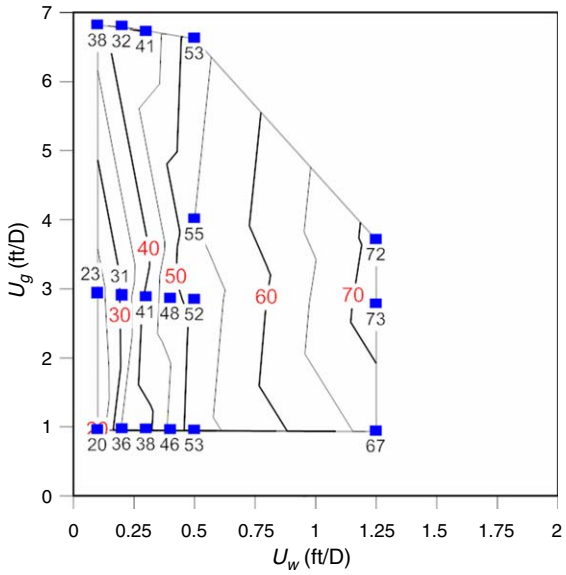

Fig. 7—Pressure gradient (in psi/ft) in the presence of oil, as a function of gas (U_g) and water (U_w) superficial velocities (in ft/D) at 35°C in a Bentheimer core of 1.98 darcies. Individual data are indicated by blue symbols. The model oil used consists of 10% OA and 90% hexadecane, coinjected with foam at a fixed U_o/U_w ratio = 1/4. Each filled symbol represents a steady-state measurement.

The high-quality regime in Fig. 7, compared with that in Figs. 5 and 6, extends to a much greater range of U_w. This suggests that the introduction of OA greatly increases S_w^*, weakening foam to a much larger extent than C_{16}. However, the ∇p contours in this regime reveal non-Newtonian behavior: ∇p depends on U_w, but not linearly. Using Darcy's law, the nonlinear dependence of ∇p on U_w in the high-quality regime indicates that the S_w^*, usually represented as a constant throughout the high-quality regime in the absence of oil, rises with increasing U_w in the presence of oil. Because oil and foam here are coinjected at a fixed U_o/U_w ratio, increasing U_w also means increasing the oil saturation, suggesting a greater destabilizing effect. However, the specific dependence of S_w^* on S_o is not clear yet because of the lack of oil-saturation data during corefloods. The decrease in apparent viscosity with increasing total superficial velocity might reflect either shear-thinning rheology or the destabilizing effect of oil on foam.

Fig. 7 also illustrates that the high-quality regime in the presence of 10 wt% OA extends down to much lower foam qualities (transition foam quality $f_g^* < 0.44$), compared with Figs. 5 and 6. This suggests a greater destabilizing effect of oil on foam than with C_{16}. For instance, $(U_w, U_g) = (0.2, 2)$ in Fig. 7 yields a ∇p of 31 psi/ft, which is nearly 13 times lower than the ∇p obtained for the same set of flow rates in Fig. 5.

LE Foam Flow With 20 wt% OA in Model Oil. **Fig. 8** shows the two foam-flow regimes with 20 wt% OA. The data are extended to lower U_g than with 10 wt% OA in Fig. 7. Both high- and low-quality regimes show modest shear-thinning behavior. However, similar to Fig. 7, the high-quality regime in Fig. 8 shifts to the right and extends to a greater range of U_w. The low-quality regime shrinks to much lower foam qualities (less than approximately 0.2). This suggests that the increase in the concentration of the more-harmful oil component in an oil mixture destabilizes foam to a greater degree.

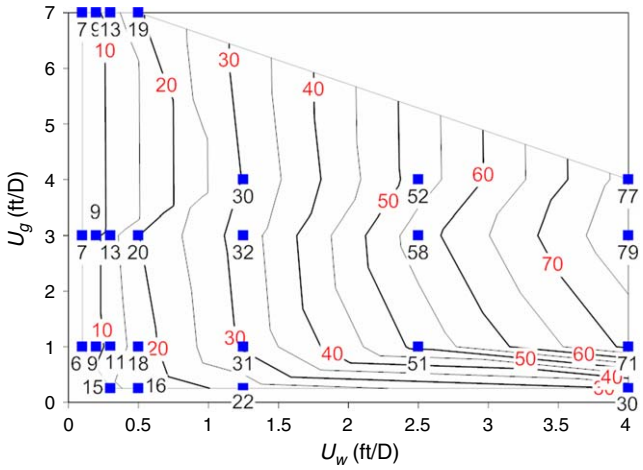

Fig. 8—Pressure gradient (in psi/ft) in the presence of oil, as a function of gas (U_g) and water (U_w) superficial velocities (in ft/D) at 35°C in a Bentheimer core of 1.98 darcies. Individual data are indicated by blue symbols. The model oil used consists of 20% OA and 80% hexadecane, coinjected with foam at a fixed U_o/U_w ratio = 1/4. Each filled symbol represents a steady-state measurement.

The maximum ∇p achieved in Fig. 8 is approximately 13.3 times lower than that without oil in Fig. 5 for same range of flow rates examined, demonstrating again that oil affects both the high- and low-quality regimes. The more detrimental effect of oil on foam in Fig. 8 clearly suggests that the high-quality regime bears greater vulnerability to oil. For instance, ∇p at $(U_w, U_g) = (2, 0.7)$, in the low-quality regime of Fig. 8, is approximately 40 psi/ft, approximately 6.8 times less than that in the absence of oil, which is 271 psi/ft in Fig. 5. However, ∇p in the high-quality regime of Fig. 8 [9 psi/ft at $(U_w, U_g) = (0.2, 2)$] is nearly 40 times less than that in Fig. 5 (400 psi/ft) for the same pair of superficial velocities.

All the experimental conditions are the same in Figs. 7 and 8 except for the oil composition. A 10-wt% increase in OA in the model oil causes a decrease in gas mobility reduction of approximately two to three times [e.g., 9 psi/ft in Fig. 8 vs. 31 psi/ft in Fig. 7 at $(U_w, U_g) = (0.2, 2)$, or 30 psi/ft in Fig. 8 vs. 67 psi/ft in Fig. 7 at $(U_w, U_g) = (1.25, 1)$]. This suggests that oil composition plays as significant a role as oil saturation on foam stability. The absence of data on oil saturation throughout our experiments makes it difficult to quantitatively compare the effect of oil saturation with that of oil composition on those two regimes. But coinjecting oil and foam at a fixed U_o/U_w ratio indicates that lower U_w also qualitatively means lower oil saturation, suggesting less destabilization of foam.

Fit of Model Parameters To Data. Simulating foam-EOR processes in contact with oil confronts many challenges (Farajzadeh et al. 2012; Rossen 2013). One striking challenge among others is which regimes are affected by oil and how oil affects those two regimes. Our experimental data demonstrate that oil affects both regimes but by a different magnitude. Specifically, oil affects the high-quality regime through its effect on limiting water saturation and the low-quality regime through its effect on gas-mobility reduction. Fitting foam-model parameters to these data provides a reference for the simulation and prediction of foam performance in the presence of oil. Note that oil saturation is difficult, if not impossible, to control during corefloods. It is not a constant in our experiments of Figs. 6, 7, and 8. One must estimate oil saturation using the oil relative permeability function, which of course introduces some uncertainty.

Model-Fit Results. Here, we present a method similar to that of Cheng et al. (2000) to fit model parameters to the data of Figs. 5 through 8. In particular, three major functions in the foam model are considered in our model fit to capture the physical effects of water saturation, oil saturation, and shear thinning on the two regimes. Essentially, one needs to fit two key parameters: the limiting water saturation S_w^*, dominating the high-quality regime, and the reference MRF *fmmob,* controlling the low-quality regime. All foam parameters in this model shift the two regimes by modifying the two key parameters. The parameter *epcap* in F_5 is used here to capture shear-thinning behavior in the low-quality regime (Eq. 5). The detailed fitting procedure applied in this study can be found in Appendix B.

Table 1 summarizes the parameter values, with and without accounting for shear thinning, fitted to the data of Figs. 5 through 8, applying the fitting procedure described in Appendix B. The representative ∇p contours for 300 psi/ft with f_g^* at $(U_w, U_g) = (0.17, 0.75)$ from Fig. 5 and for 160 psi/ft with f_g^* at $(U_w, U_g) = (0.2, 0.9)$ from Fig. 6, respectively, are illustrated in the first two figures of Appendix A. The contours plotted from Figs. 7 and 8, particularly for fitting S_w^* to each ∇p contour, are then plotted in the third and fourth figures of Appendix A. The MRF for the case with 20% OA in Appendix A is fitted using the 30-psi/ft contour with f_g^* at $(U_w, U_g) = (1.17, 0.45)$. The superscript of *fmmob** indicates that it excludes shear thinning, whereas *fmmob* is the reference MRF adjusted for shear thinning. When oil is introduced, both *fmmob** and *fmmob* incorporate the effects of oil. The model parameter *epdry*/*sfbet* is set to a large value (e.g., 20,000) to provide an abrupt transition between regimes. The assumption of an abrupt transition is justified in our data as well, as shown in the last two figures in Appendix A. The value of *fmcap* in Figs. 5 and 6 is dependent on the contour for 50 psi/ft, and in Figs. 7 and 8 on the contour for 3 psi/ft, to allow shear thinning to have an effect. The model fits to the data of Figs. 6 through 8 use the same value of *epcap* depending on the data of Fig. 5 to account for shear thinning in the low-quality regime. In other words, in our initial fit we assume that the presence of oil does not alter the shear-thinning nature of the low-quality regime.

	Fitted Parameters							
Cases	*fmmob**	F_3*	*fmmob*	F_3	*fmdry*/*sfdry*	*epdry*/*sfbet*	*epcap*	*fmcap*
Without oil	2.26×10^5	—	5.99×10^6	—	0.146	2.00×10^4	1.83	7.50×10^{-5}
C_{16}	9.73×10^4	0.431	8.18×10^5	0.137	0.148	2.00×10^4	1.83	7.50×10^{-5}
10% OA	Low-quality regime not observed				0.160 at 20 psi/ft 0.160 at 30 psi/ft 0.162 at 40 psi/ft 0.164 at 50 psi/ft 0.169 at 60 psi/ft 0.173 at 70 psi/ft	2.00×10^4	1.83	4.48×10^{-6}
20% OA	2.96×10^4	0.131	2.00×10^6	0.334	0.170 at 7 psi/ft 0.180 at 10 psi/ft 0.183 at 20 psi/ft 0.188 at 30 psi/ft 0.191 at 40 psi/ft 0.193 at 50 psi/ft 0.194 at 60 psi/ft 0.194 at 70 psi/ft	2.00×10^4	1.83	4.48×10^{-6}

Table 1—Overview of fitted parameter values using the STARS (CMG 2015) foam model for all data. The model fit assumes a large value of *epdry*/*sfbet*; we here use a value of 2×10^4.

Figs. 9 and 10 show the model fit in the absence of oil. For experiments in the presence of oil, **Figs. 11 through 16** are plotted using a combination of the dry-out model and wet-foam model to capture the effects of oil on the high- and low-quality regimes, respectively. The model fit without oil or with oil slightly destabilizing foam, as C_{16} does here, assuming a constant S_w^* throughout the high-quality regime and considering shear thinning in the low-quality regime, gives good agreement with data. However, when oil that is

substantially detrimental to foam is introduced, the model fit with the previously discussed assumptions does not show a good match to data. Instead, a better fit to data is obtained with S_w^* fitted separately to each ∇p contour in the high-quality regime and with shear thinning neglected in the low-quality regime. In other words, the presence of these oils (10 and 20 wt% OA) changes the nature of shear rheology in the low-quality regime.

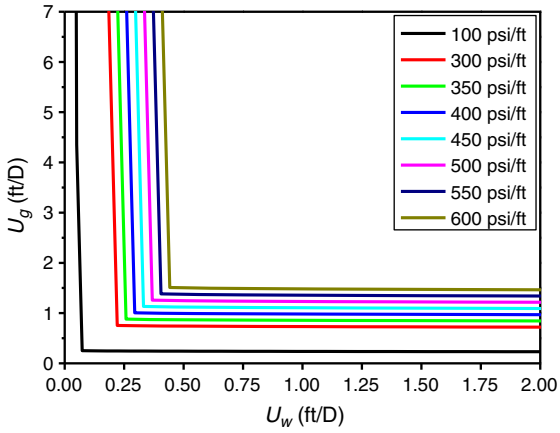

Fig. 9—Model fit to data of Fig. 5, in the absence of oil and ignoring shear thinning in the low-quality regime: *fmmob = 2.26×10^5, *fmdry* = 0.146, *epdry* = 2.00×10^4.**

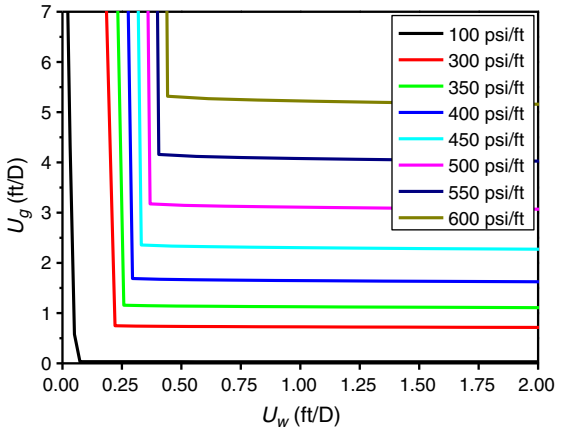

Fig. 10—Model fit to data of Fig. 5, in the absence of oil and including shear thinning in the low-quality regime: *fmmob* = 5.99×10^6, *fmdry* = 0.146, *epdry* = 2.00×10^4, *epcap* = 1.83; *fmcap* = 7.50×10^{-5}.

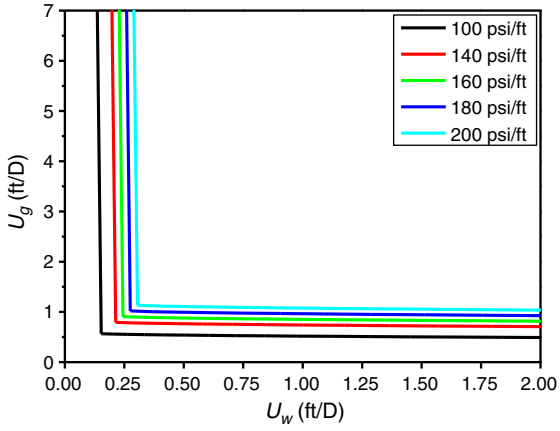

Fig. 11—Model fit to data of Fig. 6, in the presence of C_{16} and excluding shear thinning in the low-quality regime: *fmmob = 9.73×10^4, *sfdry* = 0.148, *sfbet* = 2.00×10^4.**

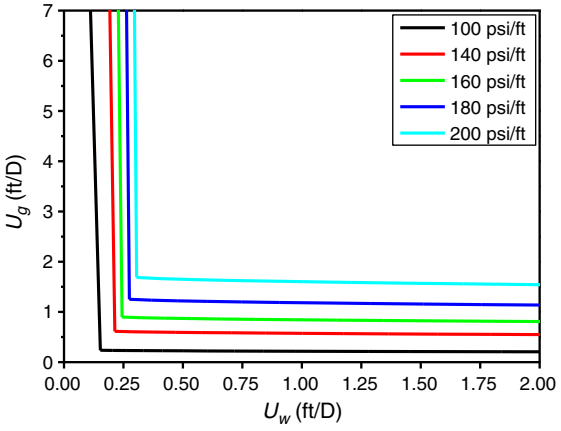

Fig. 12—Model fit to data of Fig. 6, in the presence of C_{16} and including shear thinning in the low-quality regime: *fmmob* = 8.18×10^5, *sfdry* = 0.148, *sfbet* = 2.00×10^4, *epcap* = 1.83; *fmcap* = 7.50×10^{-5}.

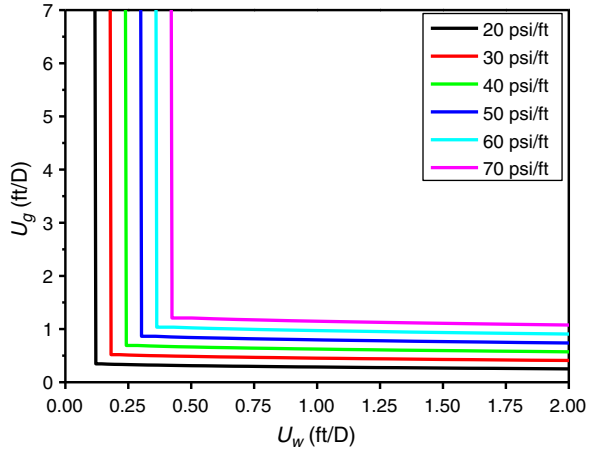

Fig. 13—Model fit to data of Fig. 7, with 10 wt% OA in model oil using a representative ∇p contour of 30 psi/ft and excluding shear thinning in the low-quality regime: *fmmob = 3.00×10^4, *sfdry* = 0.160, *sfbet* = 2.00×10^4.**

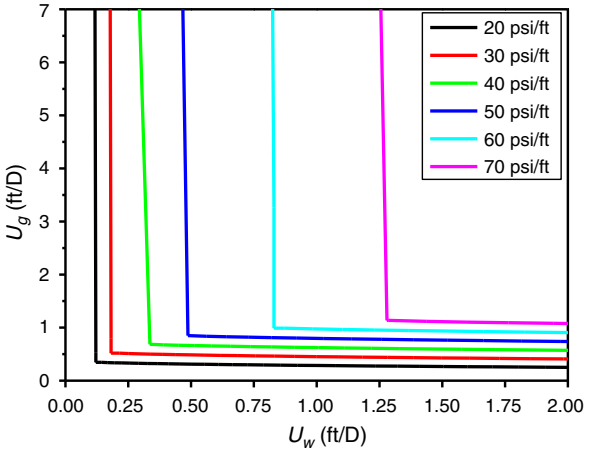

Fig. 14—Model fit to data of Fig. 7, with 10 wt% OA in model oil and excluding shear thinning in the low-quality regime: *fmmob = 3.00×10^4, *sfbet* = 2.00×10^4. Table 1 provides the limiting water saturation corresponding to each ∇p contour in the high-quality regime.**

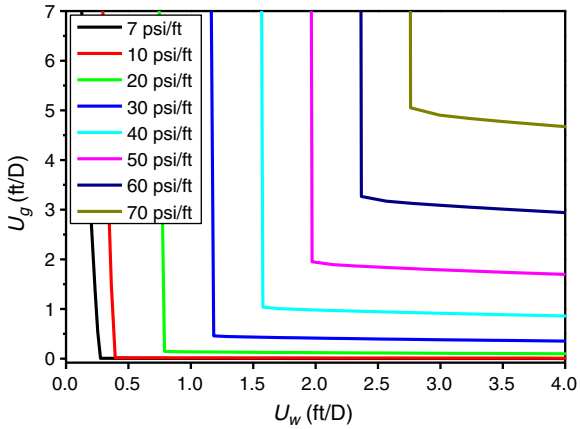

Fig. 15—Model fit to data of Fig. 8, with 20 wt% OA in model oil using a representative ∇p contour of 30 psi/ft and assuming shear thinning in the low-quality regime as fit to data without oil: *fmmob* = 2.00×10^6, *sfdry* = 0.188, *sfbet* = 2.00×10^4, *epcap* = 1.83; *fmcap* = 4.48×10^{-6}.

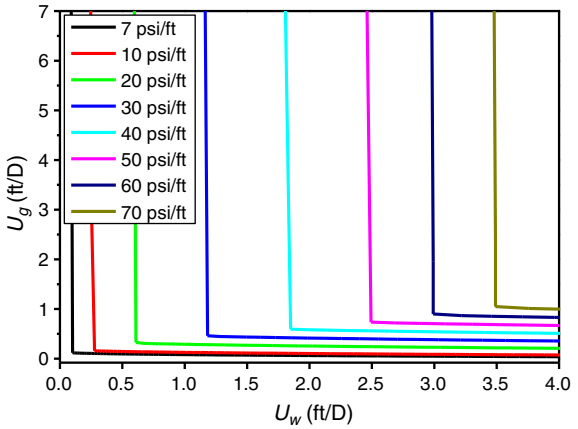

Fig. 16—Model fit to data of Fig. 8, with 20 wt% OA in model oil and excluding shear thinning in the low-quality regime: *fmmob = 2.96×10^4, *sfbet* = 2.00×10^4. Table 1 provides the values of limiting water saturation corresponding to each ∇p contour in the high-quality regime.**

Specifically, Figs. 9 through 12 illustrate that the high-quality regime fitted assuming a constant S_w^* throughout this regime shows a good agreement with the data of Figs. 5 and 6, respectively, although it does not represent the shear-thickening behavior in this regime. Fig. 9 (without considering shear thinning in the low-quality regime) and Fig. 10 (with shear thinning) demonstrate that considering shear thinning in the low-quality regime provides a much better match to the data of Fig. 5 in the absence of oil. The same conclusion can also be drawn for the model fit to data of Fig. 6 in the presence of C_{16}, which is slightly detrimental to foam. However, in both cases, either with or without oil, the fitted results fail to capture the upward-tilting ∇p contours in the low-quality regime, thereby greatly overestimating ∇p in this regime. Therefore, this issue requires the improvement of the current models to represent ∇p behavior in the low-quality regime.

Fig. 13 shows that when 10 wt% OA is introduced, the high-quality regime fitted using a fixed S_w^* fails to represent the data of Fig. 7. The assumption of a constant S_w^* throughout the high-quality regime does not apply there, in particular when the oil effect is great. Therefore, S_w^* was fitted separately to each ∇p contour in the third figure in Appendix A. The resulting model fit in Fig. 14 shows much better agreement with the data than in Fig. 13, suggesting that S_w^* here is a function either of oil saturation or of ∇p. Because of the absence of low-quality-regime data in Fig. 7, the fitted results of this regime in Figs. 13 and 14 do not reliably represent the low-quality regime.

The model fit in Fig. 15 also assumes a fixed S_w^*, showing again a great mismatch to the high-quality regime in Fig. 8. Nevertheless, in Fig. 16, fitting S_w^* depending on each specific ∇p contour in the fourth image of Appendix A agrees well with the data, suggesting again that S_w^* is a function either of ∇p or of some other properties, such as oil saturation, that depends on ∇p. Fig. 15 shows that the model fit in the low-quality regime, using the same shear-thinning fitting depending on the data without oil, does not match the data of Fig. 8. Ignoring shear thinning in this regime, as shown in Fig. 16, gives much better agreement to the data of Fig. 8 than does Fig. 15.

Attempt To Fit Oil-Related Parameters in the Model. The model fits illustrated in Figs. 13 through 16 suggest that S_w^* varies with ∇p, U_w, or U_o when OA is present. This implies that for a given oil composition, S_w^* is a function of oil saturation (S_o) and of ∇p, U_w, and/or U_o. Comparisons of the effect of oil composition must therefore be made at the same superficial velocities. At the same conditions, our data indicate that OA in the oil destabilizes foam and increases the value of S_w^*.

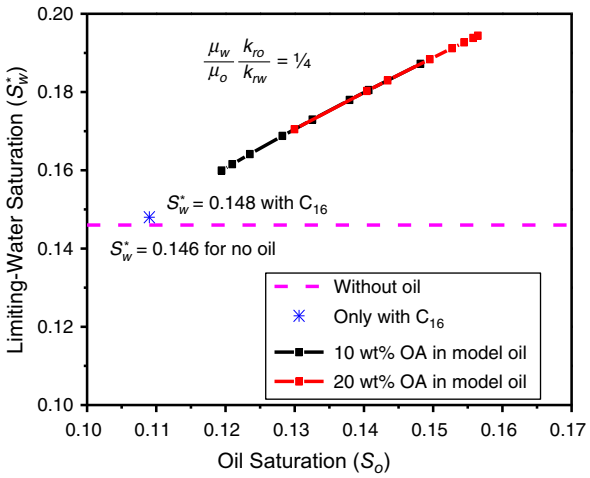

Fig. 17—The dependence of limiting water saturation (S_w^*) on oil saturation (S_o) using the data of Figs. 7 and 8. The S_o values on black and red curves are calculated using the relative permeability functions in Appendix B.

In the foam model in Eqs. 7, 8, and 9, *sfdry* (representing S_w^*) is a function of S_o. However, the constraint of $U_o/U_w = 1/4$ in our experiments also implies, through the oil/water relative permeability functions, a relation between S_w^* and S_o, because Darcy's law must be satisfied for both phases. **Fig. 17** shows our model-fitted values of S_w^* and S_o from Figs. 10, 12, 14, and 16. All the data fit on a single

curve, which suggests if one could fit the relation between S_w^* and S_o to this curve, one could represent all our results in the current model, without including oil composition, and in addition explaining the apparent non-Newtonian behavior in the high-quality regime as an indirect reflection of the dependence on oil saturation. In our model fit, we assume Corey-type relative permeability functions for oil and water. However, if the oil/water relative permeability functions are fixed and depend only on S_o and S_w, any set of data (S_o, S_w^*) at fixed U_o/U_w must lie on a single curve, such as that in Fig. 17. Thus, the trend of the results in Fig. 17 reflects the use of Corey functions and fixed U_o/U_w, not directly the effect of oil on foam.

This conclusion can be demonstrated as follows. **Fig. 18** shows a model fit to the data using Eqs. 7, 8, and 9, obtained as follows. Using any three sets of (S_o, S_w^*) data in Fig. 17, the oil-related parameters (*sloil, sfoil,* and *efoil*) in Eqs. 8 and 9 can be determined. Fitted results plotted in Fig. 18 give a good match to data in Fig. 17, but the fit is specious. **Fig. 19** shows the behavior predicted with these parameters, which differs dramatically in the high-quality regime from the data on which the model was based. The reason is as follows: Suppose one could fit the relation $U_o/U_w = 1/4$ in Fig. 17 exactly using a dry-out function $S_w^*(S_o)$ in Eqs. 8 and 9. For some superficial velocities (U_{oa}, U_{wa}) in the high-quality regime, let S_{oa} and S_{wa} be the corresponding saturations and ∇p_a the pressure gradient. Consider some multiple of ∇p_a, say $\nabla p_b = 10\ \nabla p_a$. Let S_{ob} be the oil saturation with 10 times smaller $k_{ro}(S_o)$ than S_{oa}. The dry-out function $S_w^*(S_o)$ gives a value S_{wb}, also with 10 times smaller k_{rw} than S_{wa}. The same pair of superficial velocities can be fit to a different pressure gradient—in fact, an infinite number of pressure gradients.

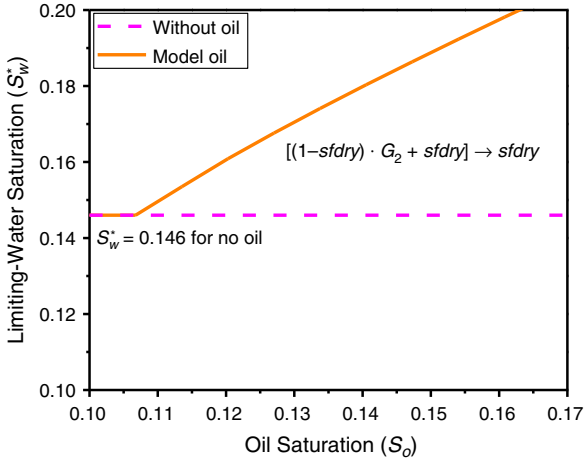

Fig. 18—Model fit to Fig. 17, using oil-related parameters in the dry-out model: *sloil* = 0.1079, *sfoil* = 1.4512, *efoil* = 0.8645.

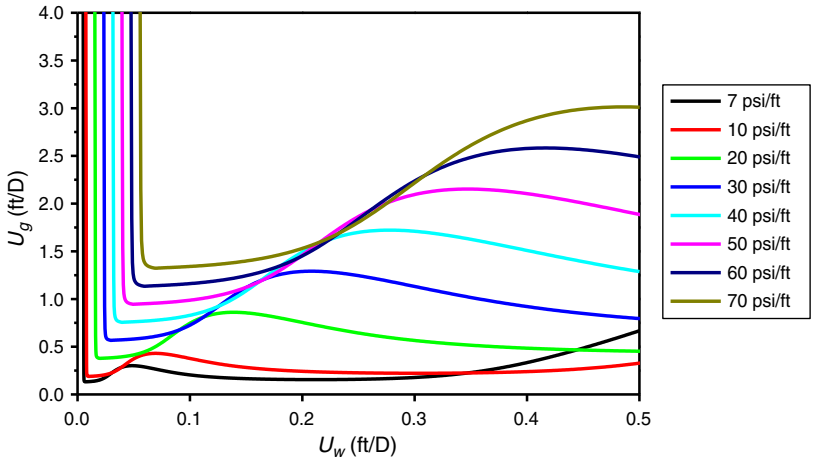

Fig. 19—Model fit to data of Fig. 8, with 20 wt% OA in model oil and excluding shear thinning in the low-quality regime: *fmmob = 2.96×10^4, *sfbet* = 2.00×10^4, *sloil* = 0.1079, *sfoil* = 1.4512, *efoil* = 0.8645. The oil-free limiting water saturation is 0.146, as suggested from Fig. 10.**

The imperfect fit in Fig. 18 to our results in Fig. 17 gives a unique solution for ∇p (Fig. 19), but one with little relation to the original data. A fit to our data for the high-quality regime must also include the effects of oil composition and possibly ∇p, U_w, or U_o.

Discussion and Remarks

This paper is paired to a study of modeling the effect of oil on foam (Tang et al. 2016). The modeling study shows how the effect of oil is represented in the current foam models. To describe the data of steady-state foam-flow dynamics with oil, both wet-foam and dry-out models are necessary to capture the effect of oil on each regime, respectively. The experimental study here provides a practical approach to quantify the effect of oil on steady-state foam behavior through its effect on the two foam regimes. The method applied for model fitting to the data is simple, and each step has a clear physical meaning. This process can give a quick but effective estimation of foam-model parameters for simulation of foam flow through porous media with oil. In a case without adequate data for the two foam

regimes, one can use a single foam-quality scan to obtain similar parameter values (Cheng et al. 2000). The good match between the fitted results and the data verifies that the model works in representing the foam behavior with oil, which is a good place to start in simulating foam displacement with oil. Because of the lack of data for oil saturation for each measurement, fitting the oil-related parameters is constrained. Therefore, to relate oil saturation to foam properties, it is recommended to run experiments with oil saturation monitored during corefloods using visualizing techniques such as computed tomography. This study works with a model oil consisting of one component less destructive to foam and the other one greatly detrimental to foam. It might suggest that the effect of lighter components in crude oil on foam is approximately an interpolation of these two components. Emulsions were observed in the effluent of the experiments with oil. It is unclear how that would affect foam stability in the corefloods. Some studies show that foam injected into a core (coinjection of surfactant solution and gas) with oil takes a significantly longer time to approach steady state than without oil. We did not find this to be the case for our experiments with coinjection of foam and oil. More efforts are still needed to investigate the fundamentals of foam dynamics with oil in porous media, either at steady state or in a dynamic process.

Conclusions

This study provides an initial approach to simulating foam EOR using steady-state data for flow in the presence of oil.

Experimental data show that the high- and low-quality regimes, central to our understanding of foam without oil, also apply in concurrent foam/oil flow. The presence of oil affects foam flow in both regimes, with the high-quality regime more vulnerable to oil. Oil composition plays as significant a role on foam flow as oil saturation.

Specifically, oil, in the high-quality regime, affects foam stability by increasing the limiting water saturation (S_w^*) below which foam collapses. In the low-quality regime, oil lessens gas-mobility reduction.

Either with or without oil, in some cases the pressure gradient (∇p) decreases with increasing water superficial velocity (U_w) at fixed gas superficial velocity (U_g). This might reflect either easier flow of bubbles under wetter conditions in the absence of oil or an increasing destabilizing effect of oil on foam with increasing U_w and U_o.

Without oil, foam flow in this study shows strongly shear-thinning behavior in the low-quality regime. This behavior changes greatly when oil is present. Foam rheology in the high-quality regime in some cases shows Newtonian behavior, but in some others shear-thickening or shear-thinning behavior.

We present an approach for fitting LE IT foam-model parameters to data for ∇p as a function of U_g and U_w, including shear thinning in the low-quality regime and the effect of oil on both regimes. To fit the data with oil, both wet-foam and dry-out models are needed to simultaneously represent each regime. Assuming a fixed S_w^* throughout the high-quality regime and including shear thinning in the low-quality regime with or without oil does not give a good match to the data, particularly when the oil effect is strong enough. In such cases, one has to fit S_w^* separately to each ∇p contour in the high-quality regime and exclude shear thinning in the low-quality regime to represent the data in both regimes.

The model fits to our data in the high-quality regime suggest that S_w^* is a function of S_o and of ∇p, U_o, or U_w. To fit our data, one must include the effects of oil composition and possibly ∇p, U_o, or U_w. None of the current foam-simulation models captures the upward-tilting ∇p contours seen in some cases in the low-quality regime.

Nomenclature

$efoil$ = oil exponent (dry-out model), dimensionless (Eq. 9)
$epcap$ = shear-thinning exponent, dimensionless (Eq. 5)
$epdry$ = water parameter in foam model (wet-foam model), dimensionless (Eq. 3)
$epoil$ = oil exponent (wet-foam model), dimensionless (Eq. 4)
f_g^* = transition-foam quality between the two regimes, fraction
$floil$ = lower limiting-oil saturation on foam (wet-foam model), dimensionless (Eq. 4)
$fmcap$ = reference capillary number, dimensionless (Eq. 5)
$fmdry$ = limiting-water saturation (wet-foam model), dimensionless (Eq. 3)
$fmmob$ = reference MRF, dimensionless (Eq. 2)
$fmoil$ = upper limiting-oil saturation on foam (wet-foam model), dimensionless (Eq. 4)
FM = MRF, dimensionless (Eq. 2)
F_1 = effect of surfactant concentration on foam, dimensionless (Eq. 2)
F_2 = effect of water saturation on foam, dimensionless (Eq. 3)
F_3 = effect of oil saturation on foam, dimensionless (Eq. 4)
F_4 = effect of gas superficial velocity on foam, dimensionless (Eq. 2)
F_5 = effect of shear-thinning rheology on foam, dimensionless (Eqs. 5 and 6)
F_6 = effect of critical capillary number on foam, dimensionless (Eq. 2)
F_7 = effect of water saturation on foam (dry-out model), dimensionless (Eq. 7)
G_2 = effect of oil saturation on foam (dry-out model), dimensionless (Eq. 9)
k = permeability, m^2
k_{ro} = oil relative permeability, dimensionless
k_{rw} = water relative permeability, dimensionless
k_{rg}^f = effective gas relative permeability with foam, dimensionless
k_{rg}^0 = foam-free gas relative permeability, dimensionless
MRF = MRF, dimensionless (Eq. 10)
N_{ca} = capillary number, dimensionless
$sfbet$ = water parameter in foam model (dry-out model), dimensionless (Eq. 7)
$sfdry$ = limiting-water saturation, dimensionless (Eq. 7)
$sfoil$ = upper limiting-oil saturation on foam (dry-out model), dimensionless (Eq. 9)
$sloil$ = lower limiting-oil saturation on foam (dry-out model), dimensionless (Eq. 9)
S_{gr} = residual gas saturation, fraction
S_{or} = residual oil saturation, fraction
S_w, S_o, S_g = water, oil, and gas saturation, respectively, fraction
S_{wc} = connate-water saturation, fraction

S_w^* = water saturation at limiting capillary pressure, fraction
T = temperature, °C
U_t = total superficial velocity, m/s
U_w, U_g, U_o = water, gas, and oil superficial velocity, respectively, m/s
Δp = pressure drop, Pa
μ_w, μ_g, μ_o = water, gas, and oil viscosity, Pa·s
σ_{wg} = water/gas surface tension, N/m
∇p = pressure gradient, Pa/m

Superscripts and Subscripts

a, b = denoting two different states
f = foam
fm = in the presence of foam
nf = in the absence of foam

Acknowledgments

This study was funded in part by the Joint Industry Project on Foam for EOR led by author William R. Rossen at Delft University of Technology, and by the China Scholarship Council. We acknowledge the recommendation of model oil used in this study by Hans Wubs. Author Sebastien Vincent-Bonnieu also thanks Shell Global Solutions International for permission to publish this article.

References

Alvarez, J. M., Rivas, H. J., and Rossen, W. R. 2001. Unified Model for Steady-State Foam Behavior at High and Low Foam Qualities. *SPE J.* **6** (3): 325–333. SPE-74141-PA. https://doi.org/10.2118/74141-PA.

Andrianov, A., Farajzadeh, R., Nick, M. M. et al. 2011. Immiscible Foam for Enhancing Oil Recovery: Bulk and Porous Media Experiments. Presented at the SPE Enhanced Oil Recovery Conference, Kuala Lumpur, 19–21 July. SPE-143578-MS. https://doi.org/10.2118/143578-MS.

Aveyard, R., Binks, B. P., Fletcher, P. D. I. et al. 1994. Aspects of Aqueous Foam Stability in the Presence of Hydrocarbon Oils and Solid Particles. *Adv. Colloid Interf. Sci.* **48** (April): 93–120. https://doi.org/10.1016/0001-8686(94)80005-7.

Basheva, E. S., Ganchev, D., Denkov, N. D. et al. 2000. Role of Betaine as Foam Booster in the Presence of Silicone Oil Drops. *Langmuir* **16** (3): 1000–1013. https://doi.org/10.1021/la990777+.

Bergeron, V., Fagan, M. E., and Radke, C. J. 1993. Generalized Entering Coefficients: A Criterion for Foam Stability Against Oil in Porous Media. *Langmuir* **9** (7): 1704–1713. https://doi.org/10.1021/la00031a017.

Boeije, C. S. and Rossen, W. 2015. Fitting Foam-Simulation-Model Parameters to Data: I. Coinjection of Gas and Liquid. *SPE Res Eval & Eng* **18** (2): 264–272. SPE-174544-PA. https://doi.org/10.2118/174544-PA.

Cheng, L., Reme, A. B., Shan, D. et al. 2000. Simulating Foam Processes at High and Low Foam Qualities. Presented at the SPE/DOE Improved Oil Recovery Symposium, Tulsa, 3–5 April. SPE-59287-MS. https://doi.org/10.2118/59287-MS.

Computer Modelling Group (CMG). 2015. STARS User's Guide, Version 2015. Calgary: Computer Modelling Group.

de Vries, A. S. and Wit, K. 1990. Rheology of Gas/Water Foam in the Quality Range Relevant to Steam Foam. *SPE Res Eng* **5** (2): 185–192. SPE-18075-PA. https://doi.org/10.2118/18075-PA.

Eftekhari, A. A. and Farajzadeh, R. 2017. Effect of Foam on Liquid Phase Mobility in Porous Media. *Scientific Reports* **7** (March): 43870. https://doi.org/10.1038/srep43870.

Elliott, C., Vijayakumar, V., Zink, W. et al. 2007. National Instruments LabVIEW: A Programming Environment for Laboratory Automation and Measurement. *SLAS Technology: Translating Life Sciences Innovation* **12** (1): 17–24. https://doi.org/10.1016/j.jala.2006.07.012.

Farajzadeh, R., Andrianov, A., Krastev, R. et al. 2012. Foam–Oil Interaction in Porous Media: Implications for Foam Assisted Enhanced Oil Recovery. *Adv. Colloid Interf. Sci.* **183–184** (15 November): 1–13. https://doi.org/10.1016/j.cis.2012.07.002.

Fisher, A. W., Foulser, R. W. S., and Goodyear, S. G. 1990. Mathematical Modeling of Foam Flooding. Presented at the SPE/DOE Enhanced Oil Recovery Symposium, Tulsa, 22–25 April. SPE-20195-MS. https://doi.org/10.2118/20195-MS.

Friedmann, F., Chen, W. H., and Gauglitz, P. A. 1991. Experimental and Simulation Study of High-Temperature Foam Displacement in Porous Media. *SPE Res Eng* **6** (1): 37–45. SPE-17357-PA. https://doi.org/10.2118/17357-PA.

Harkins, W. D. and Feldman, A. 1922. Films: The Spreading of Liquids and the Spreading Coefficient. *J. Am. Chem. Soc.* **44** (12): 2665–2685. https://doi.org/10.1021/ja01433a001.

Hirasaki, G. J. and Lawson, J. B. 1985. Mechanisms of Foam Flow in Porous Media: Apparent Viscosity in Smooth Capillaries. *SPE J.* **25** (2): 176–190. SPE-12129-PA. https://doi.org/10.2118/12129-PA.

Islam, M. R. and Farouq Ali, S. M. 1988. Numerical Simulation of Foam Flow in Porous Media. Presented at the Annual Technical Meeting, Calgary, 12–16 June. PETSOC-88-39-04. https://doi.org/10.2118/88-39-04.

Kam, S. I., Nguyen, Q. P., Li, Q. et al. 2007. Dynamic Simulations With an Improved Model for Foam Generation. *SPE J.* **12** (1): 35–48. SPE-90938-PA. https://doi.org/10.2118/90938-PA.

Kim, J., Dong, Y., and Rossen, W. R. 2005. Steady-State Flow Behavior of CO_2 Foam. *SPE J.* **10** (4): 405–415. SPE-89351-PA. https://doi.org/10.2118/89351-PA.

Kovscek, A. R., Patzek, T. W., and Radke, C. J. 1995. A Mechanistic Population Balance Model for Transient and Steady-State Foam Flow in Boise Sandstone. *Chem. Eng. Sci.* **50** (23): 3783–3799. https://doi.org/10.1016/0009-2509(95)00199-F.

Kular, G. S., Lowe, K., and Coombe, D. 1989. Foam Application in an Oil Sands Steamflood Process. Presented at the SPE Annual Technical Conference and Exhibition, San Antonio, Texas, 8–11 October. SPE-19690-MS. https://doi.org/10.2118/SPE-19690-MS.

Law, D. H.-S., Yang, Z.-M., and Stone, T. W. 1992. Effect of the Presence of Oil on Foam Performance: A Field Simulation Study. *SPE Res Eng* **7** (2): 228–236. SPE-18421-PA. https://doi.org/10.2118/18421-PA.

Mannhardt, K., Novosad, J. J., and Schramm, L. L. 1998. Foam/Oil Interactions at Reservoir Conditions. Presented at the SPE/DOE Improved Oil Recovery Symposium, Tulsa, 19–22 April. SPE-39681-MS. https://doi.org/10.2118/39681-MS.

Mohammadi, S. S., Coombe, D. A., and Stevenson, V. M. 1993. Test of Steam-Foam Process for Mobility Control in South Casper Creek Reservoir. *J Can Pet Technol* **32** (10): 49–54. PETSOC-93-10-06. https://doi.org/10.2118/93-10-06.

Myers, T. J. and Radke, C. J. 2000. Transient Foam Displacement in the Presence of Residual Oil: Experiment and Simulation Using a Population-Balance Model. *Ind. Eng. Chem. Res.* **39** (8): 2725–2741. https://doi.org/10.1021/ie990909u.

Osterloh, W. T. and Jante, M. J. 1992. Effects of Gas and Liquid Velocity on Steady-State Foam Flow at High Temperature. Presented at the SPE/DOE Enhanced Oil Recovery Symposium, Tulsa, 22–24 April. SPE-24179-MS. https://doi.org/10.2118/24179-MS.

Patzek, T. W. and Myhill, N. A. 1989. Simulation of the Bishop Steam Foam Pilot. Presented at the SPE California Regional Meeting, Bakersfield, California, 5–7 April. SPE-18786-MS. https://doi.org/10.2118/18786-MS.

Reme, A. B. 1999. *Parameter Fitting and Calibration Study With a Commercial Foam Simulator*. PhD dissertation, Norwegian University of Science and Technology, Trondheim, Norway.

Rossen, W. R. 1996. Foams in Enhanced Oil Recovery. In *Foams: Theory, Measurements, and Applications*, ed. R. K. Prud'homme and S. A. Khan, 413–464. New York City: Marcel Dekker.

Rossen, W. R. 2013. Numerical Challenges in Foam Simulation: A Review. Presented at the SPE Annual Technical Conference and Exhibition, New Orleans, 30 September–2 October. SPE-166232-MS. https://doi.org/10.2118/166232-MS.

Rossen, W. R., Zeilinger, S. C., Shi, J. X. et al. 1999. Simplified Mechanistic Simulation of Foam Processes in Porous Media. *SPE J.* **4** (3): 279–287. SPE-57678-PA. https://doi.org/10.2118/57678-PA.

Schramm, L. L. and Novosad, J. J. 1990. Micro-Visualization of Foam Interactions With a Crude Oil. *Colloid. Surface.* **46** (1): 21–43. https://doi.org/10.1016/0166-6622(90)80046-7.

Schramm, L. L. and Novosad, J. J. 1992. The Destabilization of Foams for Improved Oil Recovery by Crude Oils: Effect of the Nature of the Oil. *J. Pet. Sci. Eng.* **7** (1–2): 77–90. https://doi.org/10.1016/0920-4105(92)90010-X.

Simjoo, M. and Zitha, P. L. J. 2013. Effects of Oil on Foam Generation and Propagation in Porous Media. Presented at the SPE Enhanced Oil Recovery Conference, Kuala Lumpur, 2–4 July. SPE-165271-MS. https://doi.org/10.2118/165271-MS.

Spirov, P., Rudyk, S., and Khan, A. 2012. Foam Assisted WAG: Snorre Revisit With New Foam Screening Model. Presented at the North Africa Technical Conference and Exhibition, Cairo, 20–22 February. SPE-150829-MS. https://doi.org/10.2118/150829-MS.

Tang, J., Ansari, M. N., and Rossen, W. R. 2016. Modelling the Effect of Oil on Foam for EOR. Presented at ECMOR XV–15th European Conference on the Mathematics of Oil Recovery, Amsterdam, 29 August–1 September. https://doi.org/10.3997/2214-4609.201601877.

Zanganeh, M. N., Kam, S. I., LaForce, T. et al. 2011. The Method of Characteristics Applied to Oil Displacement by Foam. *SPE J.* **16** (1): 8–23. SPE-121580-PA. https://doi.org/10.2118/121580-PA.

Appendix A—Figures Adapted for Model Fit

Following the method of Cheng et al. (2000), we use a contour of fixed ∇p passing through the low- and high-quality regimes to fit S_w^* and *fmmob**. **Figs A-1 through A-6** show the contours used in each case. See Appendix B for details of the fitting procedure.

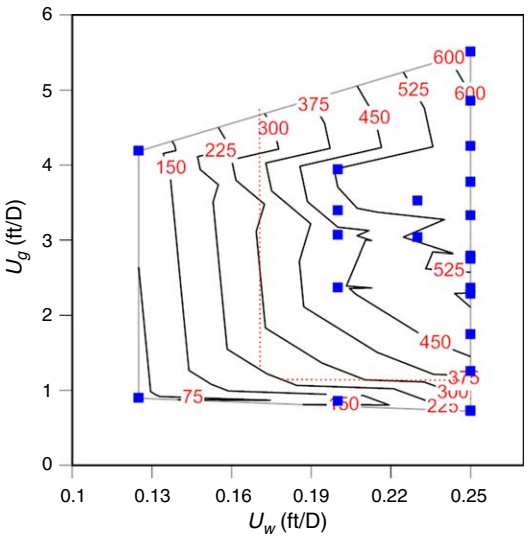

Fig. A-1—Expanded view of Fig. 5, with representative contour at 300 psi/ft (red dotted lines) used in fitting the model to data.

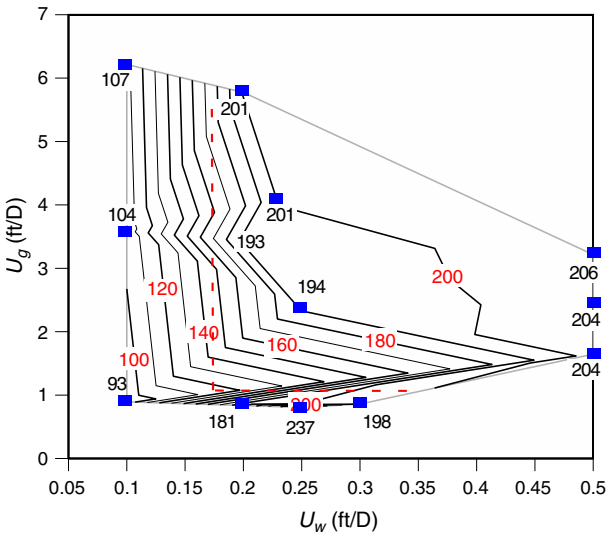

Fig. A-2—Expanded view of Fig. 6, with representative contour at 160 psi/ft (red dotted lines) used in fitting the model to data.

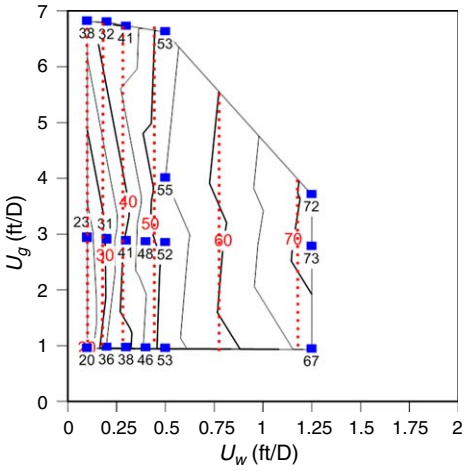

Fig. A-3—Contours of fixed ∇p from Fig. 7 used in fitting the model to data. Each red dotted line represents a specific ∇p contour across the high-quality-regime data.

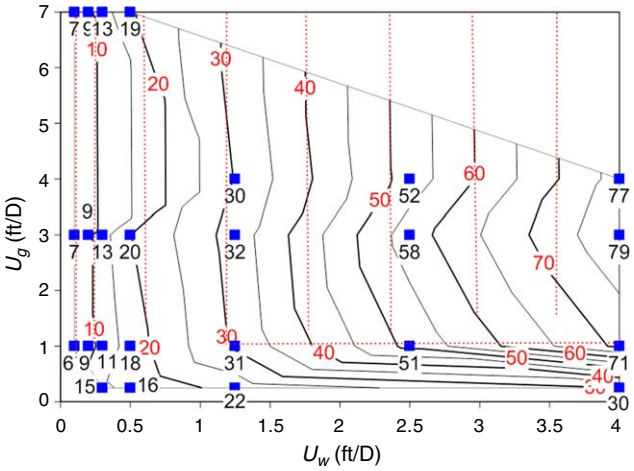

Fig. A-4—Contours of fixed ∇p from Fig. 8 used in fitting the model to data. Each red dotted line represents a specific ∇p contour across the data in each regime.

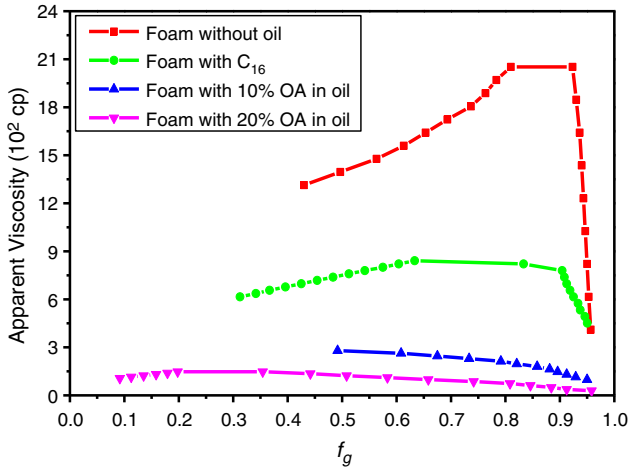

Fig. A-5—Comparison of oil-compositional effect on LE foam strength in terms of single foam-quality scan. The data are adapted from Figs. 5, 6, 7, and 8 by making a diagonal line at fixed $U_t = 3$ ft/D.

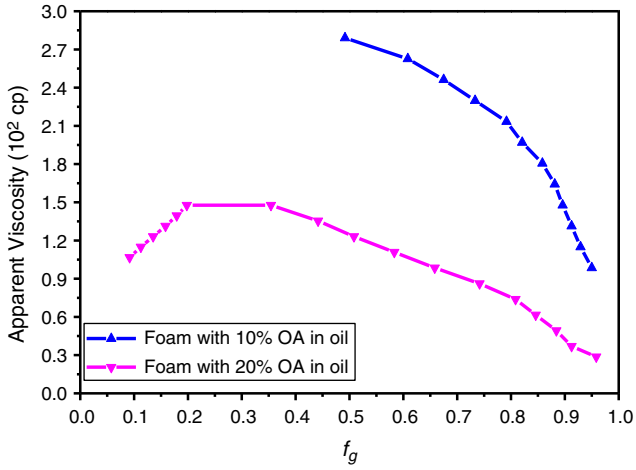

Fig. A-6—An expanded view of Fig. A-5 for illustration of foam-quality transition with OA in model oil.

Appendix B—Procedure for Fitting Model Parameters To Data

The functions examined in the foam model include the following parameters: *fmmob, fmdry* (*sfdry*), *epdry* (*sfbet*), *epcap, fmcap, floil* (*sloil*), *fmoil* (*sfoil*), and *epoil* (*efoil*). However, because of the absence of oil-saturation data in our experiments, it is not feasible to fit all the oil-related parameters separately. Therefore, five parameters in total are fitted in this study: *fmmob, fmdry* (*sfdry*), *epdry* (*sfbet*), *epcap,* and *fmcap*. Comparing *fmmob* in the absence of oil with that incorporating the effect of oil when foam concurrently flows with oil gives the value of function F_3. Similarly, comparison of *fmdry* in the absence of oil and *sfdry* altered by oil yields the value of function G_2. The values of F_3 and G_2, respectively, reflect the effects of oil on foam strength in the low-quality regime and foam stability in the high-quality regime (Eqs. 2, 4, 7, and 8).

Reme (1999) and Cheng et al. (2000) have sketched the parameter-fitting procedures for the STARS and University of Texas foam models (Rossen et al. 1994; CMG 2015), respectively, without including the effect of oil. Here, we use a method similar to that of Cheng et al. (2000) to fit model parameters to data, including the effects of oil on *fmmob* and *fmdry* (*sfdry*). Before fitting the parameters, one must specify foam-free relative permeability functions for each phase. We here use the Corey relative permeability model and the relative permeability data of Eftekhari and Farajzadeh (2017) for Bentheimer Sandstone using the same type of surfactant and the same concentration. **Table B-1** summarizes the fluid and transport properties used throughout the parameter fitting.

Quantities	Parameter Values
Water viscosity, μ_w	0.7×10^{-3} Pa·s
Gas viscosity, μ_g	2.07×10^{-5} Pa·s
Oil viscosity, μ_o	5×10^{-3} Pa·s
Water relative permeability, $k_{rw}(S_w)$	$0.713\left(\frac{S_w-0.135}{0.665-S_{or}}\right)^{2.46}$
Gas relative permeability, $k_{rg}(S_g)$	$0.94\left(\frac{S_g-0.2}{0.665-S_{or}}\right)^{1.3}$
Oil relative permeability, $k_{ro}(S_o)$	$0.5\left(\frac{S_o-S_{or}}{0.665-S_{or}}\right)^{2}$
Water/gas surface tension, σ_{wg}	0.03 N/m
Temperature, T	35°C

Table B-1—Fluid and transport properties in porous media. When oil is present, $S_{or}=0.1$; otherwise, $S_{or}=0$.

Specifically, one can fit model parameters to data following the step-by-step procedure as described here. A major advantage of this method is that each step has a clear physical meaning.

Step 1. Draw $\bigtriangledown p$ contours. For efficiently fitting parameters, one might need to smooth the $\bigtriangledown p$ contours. Then, pick up one reprehensive $\bigtriangledown p$ contour and draw vertical and horizontal straight lines, which can best represent the data in the high- and low-quality regimes, respectively, for this contour, as illustrated in **Fig. B-1** and Appendix A.

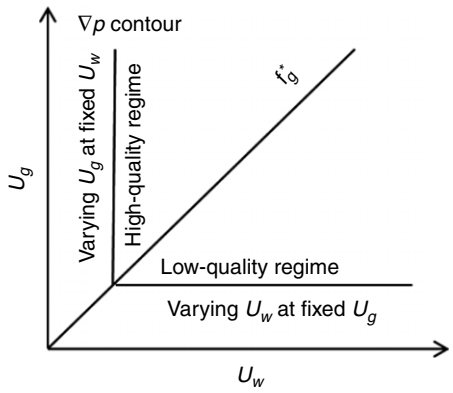

Fig. B-1—Schematic of contour treatment in each regime for fitting the model parameters to data, adapted from Cheng et al. (2000).

This approach assumes that the $\bigtriangledown p$ contours in the low-quality regime are horizontal. However, in some cases, including this study, the $\bigtriangledown p$ contours in the low-quality regime with or without oil tilt upward with increasing U_w (as in Figs. 5 and 6) (Kim et al. 2005). This means that the fitted results could mismatch the low-quality-regime data, especially for higher ranges of U_w. However, none of the current foam-simulation models captures this behavior in the absence of oil. Therefore, it is necessary to improve current foam models to capture this upward-tilting $\bigtriangledown p$ trend for effectively fitting the low-quality regime. This is beyond the scope of this study. Here, we apply horizontal contours to represent low-quality-regime data throughout the model fitting. Figs. A-1 through A-4 illustrate the representative contours drawn through the data in both regimes in each case.

Step 2. Determine the limiting water saturation S_w^*. The vertical line in Fig. B-1, representing the high-quality-regime data on the representative $\bigtriangledown p$ contour, corresponds to a specific value of U_w. Applying Darcy's law for the water phase (Eq. B-1) at this value of U_w, along with $k_{rw}(S_w)$ from Table 2, yields the limiting water saturation S_w^*,

$$U_w=\frac{kk_{rw}(S_w^*)}{\mu_w}\nabla p. \quad \text{(B-1)}$$

Step 3. Calculate the reference MRF *fmmob** (the asterisk denotes the factor without considering shear thinning). As shown in Fig. B-1, the vertical and the horizontal lines intersect at one point, which marks the transition between regimes. Foam quality at this point, defined as $U_g/(U_g+U_w)$ in the absence of oil or $U_g/(U_g+U_w+U_o)$ in the presence of oil, is defined as the transition-foam quality f_g^*. The parameter *fmmob** is assumed to be constant throughout the low-quality regime. This assumption also applies at f_g^*. Applying Darcy's law to the gas phase (Eq. B-2) at f_g^* using $k_{rg}(S_g)$ from Table 2 with S_w^* known from Step 2 gives *fmmob**,

$$U_g=\frac{kk_{rg}^0(S_w^*)\dfrac{1}{1+fmmob^*}}{\mu_g}\nabla p, \quad \text{(B-2)}$$

where $k^0_{rg}(S^*_w)$ is the foam-free gas relative permeability at f^*_g, at which S^*_w is already known from Step 2. The value of *fmmob** obtained here neglects shear thinning in the low-quality regime. This is considered in Step 7.

Step 4. Set *epdry* to a large value (e.g., 20,000). The parameter *epdry* controls the abruptness of foam collapse as S_w decreases toward S^*_w. Consistent with our experimental data (e.g., Fig. 5), an abrupt transition is assumed as in the model-fitting procedure of Cheng et al. (2000).

Step 5. Specify a reference capillary number *fmcap*. As shown in Eq. 5, no matter what value of *fmcap* is used in models, F_5 must be less than unity for shear thinning to have effect. The parameter *fmcap* in this study is calculated using Eq. 6, depending on a value of ∇p smaller than all measured data in each case.

Step 6. Capture shear thinning in the low-quality regime through *epcap*. The model proposed by Rossen et al. (1994) characterizes shear thinning in the low-quality regime using $\sigma > 1$. The slope of a plot of $\log(\nabla p)$ vs. $\log(U_g)$ is σ. The parameter *epcap* here can be obtained using

$$\sigma \approx \frac{1}{1+epcap}. \quad \text{(B-3)}$$

Plotting $\log(\nabla p)$ vs. $\log(U_g)$ using the data of Fig. 5 at $U_w = 0.75$ ft/D, as illustrated in **Fig. B-2,** gives a slope of 0.3535. Then, *epcap* is 1.83 from Eq. B-3.

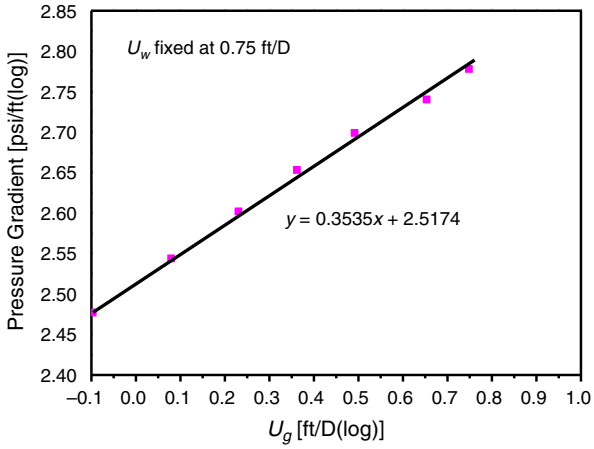

Fig. B-2—Log-log plot for ∇p vs. U_g using the data of Fig. 5, at fixed $U_w = 0.75$ ft/D.

Step 7. Adjust the reference MRF *fmmob* accounting for shear thinning. When considering shear thinning in the low-quality regime, the value of *fmmob** obtained previously is the mobility reduction that incorporates the effect of shear thinning. The model parameter *fmmob* can be obtained from *fmmob** using Eq. B-4, with *fmcap* and *epcap* obtained in Steps 5 and 6, depending on ∇p of the representative ∇p contour:

$$fmmob^* = fmmob \times \left(\frac{fmcap}{N_{ca}}\right)^{epcap}, \quad \text{(B-4)}$$

where N_{ca} is calculated from Eq. 6 using the value of ∇p from the characteristic ∇p contours.

Step 8. Fit the effect of oil through functions F_3 and G_2. As shown in Figs. 6, 7, and 8, oil affects both high- and low-quality regimes, respectively, through its effect on S^*_w and the reference MRF *fmmob* in each regime. Experimental data here suggest that oil has different magnitudes of effects on those two regimes, with the high-quality regime being more susceptible to its influence. Therefore, oil-related parameters should be fitted separately, depending on the data in each regime.

Specifically when oil is present, Steps 2 and 3 provide S^*_w and *fmmob**, each of which now incorporates the effect of oil. Using the fitted values of S^*_w and *fmmob** in Fig. 5 obtained in the absence of oil, applying Eq. 8 yields the value of G_2 in the dry-out model, accounting for the overall effect of oil on the S^*_w. The parameter *fmmob** obtained in the presence of oil, divided by the value of *fmmob** obtained in the absence of oil, gives the value of F_3 in wet-foam model, accounting for the effect of oil on gas-mobility reduction in the low-quality regime. However, the nonlinearly distributed contours in the high-quality regime of Figs. 7 and 8 suggest that S^*_w is not fixed throughout the high-quality regime, but varies with superficial velocity. Therefore, to fit the high-quality-regime data in the presence of oil, one might have to fit S^*_w corresponding to each ∇p contour in the high-quality regime, instead of just fitting one representative ∇p contour. The nonlinear spacing of contours in the low-quality regime is fit by adjusting *epcap* for oil, but observed behavior might reflect both shear thinning and the effect of oil. The fit to *epcap* in the absence of oil might not apply when oil flows with foam.

Step 9. Plot the fitted results using model-parameter values and compare with data. The experimental data demonstrate clearly that oil shifts both regimes. However, the modeling study of Tang et al. (2016) suggests that oil in the wet-foam model affects only the low-quality regime, whereas in the dry-out model, it shifts only the high-quality regime. Therefore, the wet-foam and dry-out models are both needed to represent low- and high-quality-regime data.

Jinyu Tang has been a PhD degree researcher at Delft University of Technology, The Netherlands, since 2014. He holds a master's degree in petroleum engineering from China University of Petroleum. Tang's research interests include foams for EOR, modeling of complex fluid flow through porous media, multiobjective computed tomography corefloods, and fractional-flow analysis of multiphase flow. He has been an SPE member since 2014.

Sebastien Vincent-Bonnieu is a reservoir engineer at Shell Global Solutions International and a researcher at Delft University of Technology. His current research interests include gas and surfactant EOR.

William R. Rossen is a professor of reservoir engineering at the Department of Geoscience and Engineering at Delft University of Technology. His current research concerns the use of foams for diverting fluid flow in porous media, modeling complex transport processes in networks, and understanding flow in naturally fractured geological formations. Rossen was named Best Instructor at Delft University of Technology in 2011, and was named an IOR Pioneer at the 2012 SPE/DOE Symposium on Improved Oil Recovery, in Tulsa. He is an SPE Distinguished Member.